Nanopropeller arrays of zinc oxide

Pu Xian Gao and Zhong L. Wang[a)]
School of Materials Science and Engineering, Georgia Institute of Technology, Atlanta, Georgia 30332-0245

(Received 8 December 2003; accepted 2 February 2004)

Polar surface dominated ZnO nanopropeller arrays were synthesized by a two-step high temperature solid-vapor deposition process. The axis of the nanopropellers is a straight nanowire along the *c* axis and enclosed by {2110} surfaces, which grew first; the sixfold symmetric nanoblades are later formed along the crystallographic equivalent *a* axes (⟨2110⟩) perpendicular to the nanowire; and the array is formed by epitaxial growth of nanoblades on the nanowire. The top surface of the nanoblade is the Zn terminated $+c$ plane, showing surface steps and possible secondary growth of nanowires due to higher self-catalytic activity, while the back surface is the oxygen-terminated $-c$ plane, which is smooth and inert. © *2004 American Institute of Physics.* [DOI: 10.1063/1.1702137]

Wurtzite structured ZnO, a key transparent semiconducting oxide, has versatile properties that are important for applications in electrical, optoelectronic, photovoltaic devices, and sensors.[1–5] Quasi-one-dimensional nanostructures of ZnO, such as nanowires, nanobelts, and nanotubes[6–8] are attracting much interest for their properties and potential applications in nanotechnology. A combination of the three types of fast growth directions (⟨2110⟩, ⟨0110⟩, and [0001]) and the three area-adjustable facets ({2110}, {0110}, and {0001}) of ZnO results in a diverse group of hierarchical and intricate nanostructures.[9–11] In addition to the noncentral symmetry, the semiconducting and piezoelectric as well as surface polarization characteristics of ZnO enable it to be one of the most exciting oxide nanostructures for investigating nanoscale physical and chemical properties. Structural configurations such as nanojunction arrays,[9–11] piezoelectric nanobelt,[12,13] nanospring,[12] nanoring,[13] etc, have been reported. In this letter, we report a new nanostructure for ZnO: nanopropeller arrays. The structure and growth process of the nanopropellers will be presented. The effect of temperature gradient and polar surfaces on the growth structure will be elaborated. The structure reported here could have applications for sensing, microfluidics, electromechnical coupled devices, and transducers.

The polar surface dominated nanopropeller arrays of ZnO in this work were grown by a two-step high temperature solid-vapor deposition process. The experimental setup consists of a horizontal high temperature tube furnace of length ~50 cm, an alumina tube (~75 cm in length), a rotary pump system, and a gas controlling system. Commercial (Alfa Aesor) ZnO and SnO_2 powders as well as graphite with molar ratio of 3:4:1.5 were mixed, ground and then loaded on an alumina boat and positioned at the center of the alumina tube. The evaporation was conducted at 1100 °C for 60 min (step I) and then up to 1300 °C for half an hour (step II) under pressure of 200 mbar. The N_2 carrier gas flow rate is controlled at 20 sccm (standard cubic centimeters per minute). The nanopropeller arrays grew on a polycrystalline Al_2O_3 substrate in a temperature zone in the range of 600–700 °C and 800–900 °C corresponding to steps I and II, respectively.

Figure 1(a) shows a top view of the well-aligned ZnO nanopropeller arrays on a polycrystalline Al_2O_3 substrate grown in a relatively higher temperature zone [~680 °C (step I)]. Each column of nanopropeller arrays consists of six arrays of triangular shaped blades of 4–5 μm in length, and a propeller arrays of diameter ~10 μm. Columns of the nanopropellers remain their sixfold arrays of parallel nanoribbon blades around the central nanowire [Fig. 1(b)]. There is a small Sn ball of a diameter ~50 nm at the tip of the blade, which is less than half of the average width of the

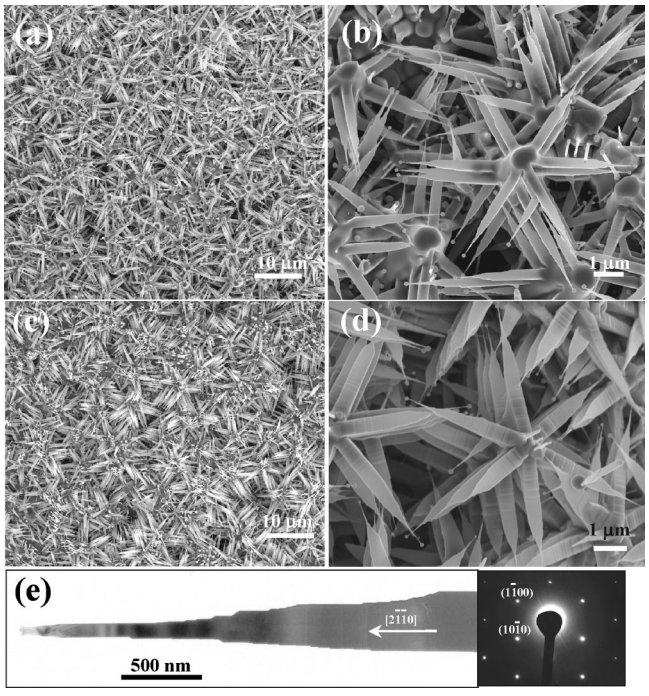

FIG. 1. (a) SEM image of bunches of ZnO nanopropeller arrays rooted at Al_2O_3 substrate; (b) magnified image of the sixfold symmetrical ZnO nanopropeller arrays with flat top surfaces; (c) nanopropeller arrays with stepped rough top surface; (d) high magnification SEM images of nanopropeller arrays with stepped rough top surface, on which there are normal oriented nanowires along the central axis; (e) TEM image of a nanopropeller blade, showing a stepped surface. The corresponding electron diffraction shows the nanoblade is along [0001] and growth direction [2110].

a)Author to whom correspondence should be addressed; electronic mail: zhong.wang@mse.gatech.edu

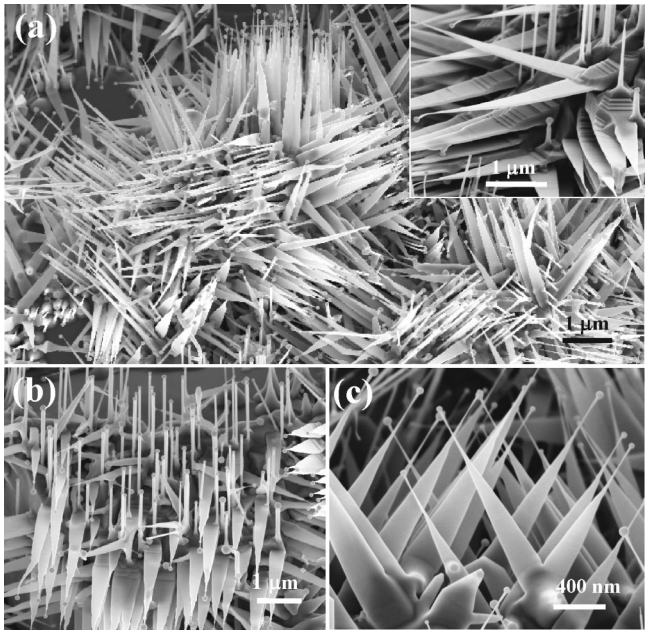

FIG. 2. (a) SEM image of the as-synthesized ZnO nanostructures, showing arrays of nanowires and nanopropeller blades. Inserted image shows surface steps at the root of the nanoblades; (b) side view of a bunch of aligned ZnO nanopropeller blades with perpendicularly ordered ZnO nanowires; and (c) top view of 60° crossed nanopropeller blades.

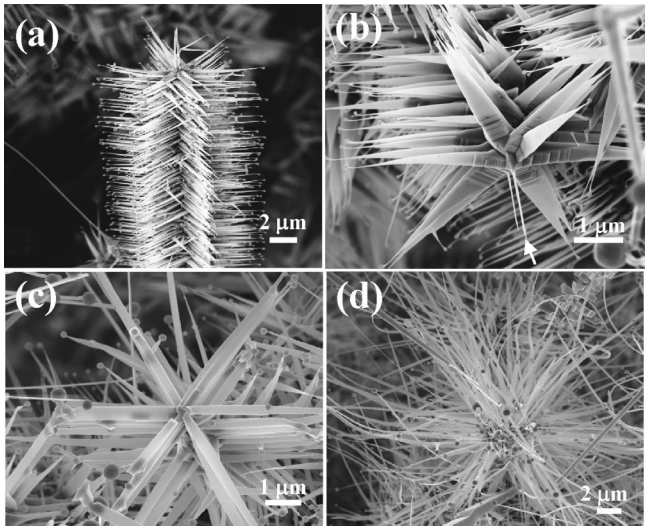

FIG. 3. Temperature dependence of the grown nanopropeller arrays: (a) SEM image of a single column of the as-synthesized ZnO nanopropeller arrays; (b) front view of a column of ZnO nanopropeller arrays with nanowires at the central axis, which was collected from a lower temperature zone (~620 °C in step I); (c) a column of ZnO nanopropeller arrays with uniform nanoribbon shape and smoother surface, which was collected from a medium temperature zone (~650 °C in step I); (d) a column of ZnO nanopropeller arrays with long nanoribbons, which was collected from a higher temperature zone (~680 °C in step I).

blade (~400 nm). All of the blades have a uniform isosceles triangular shape. Figure 1(c) gives a typical morphology of the other type of ZnO nanopropeller arrays grown on an alumina substrate. With a similar sixfold symmetry and branching phenomena as for the first case in Figs. 1(a) and 1(b), a magnified image of the nanopropeller arrays in Fig. 1(d) shows some rougher stepped top surfaces of the blades than the flat smooth surfaces as observed in Fig. 1(b). Unlike the previous case with a bare flat node at the tip of the central axis, there are several fine nanowires sticking out of the growth front. The contrast in a TEM image recorded from a nanoblade reveals that the blade always has a stepped surface [Fig. 1(e)], consistent to the SEM observation. The corresponding electron diffraction pattern indicates that the blade surfaces are $\pm(0001)$, and growth direction [2110] (a axis).

Figure 2(a) shows nanopropeller arrays grown in a lower temperature zone (600–650 °C, step I), and each column is as large as 2–5 μm in diameter. There are aligned nanowires and isosceles triangular-shape nanoblades growing perpendicularly. Fine nanowires (~50 nm in diameter) grow vertically on the top surface of the nanoblades [Fig. 2(b)] (note: the wires are only grown on one side of the nanoblades). The nanoblades are at 60° angle, corresponding to the sixfold symmetry in the c plane [Fig. 2(c)]. Uniform Sn particles of 50 nm in size are located at the tip of the nanoblades, and they are eight times smaller than the largest width of the nanoblade. Magnified side view of the nanoblades presents their rectangular cross section, as inserted in Fig. 2(a). The smallest width of the triangular-shape nanoblade is ~20 nm and the maximum width is ~500 nm. The nanoblade has a stepped top surface towards the growth direction, while the surface against the growth direction is smooth. A closer examination at the junction between the nanoblades and the axial nanowire shows major steps.

In addition to the closely packed columns of nanopropeller arrays, freestanding nanopropeller arrays have also been found. Figure 3(a) is a side view of a single column of freestanding ZnO nanopropeller arrays formed at relatively low temperature region [~620 °C (step I)], which is apparently composed of hexagonal symmetrical arrays of ZnO triangular-shape blade of 20–500 nm in width and 4–5 μm in length. There are two nanowires standing out at the tip of the symmetry axis, as indicated by an arrow in Fig. 3(b).

Different from the triangular-shaped nanoblades presented in the sample grown in a lower temperature zone [Fig. 3(b)], nanoblades with uniform widths are found in a medium temperature zone [Fig. 3(c)] [~650 °C (step I)]. In a higher temperature zone [~680 °C (step I)], the nanoblades are long and curved [Fig. 3(d)].

The top and bottom surfaces of the nanoblades have different surface morphology. Figure 4(a) is a closer side view of the top surfaces of two nanoblades, showing steps perpendicular to the blade direction of [2110]. The steps are responsible for the increased blade thickness approaching the root. The bottom surface of the nanoblades is flat and much smoother [Fig. 4(b)]. A broken blade reveals its trapezoid

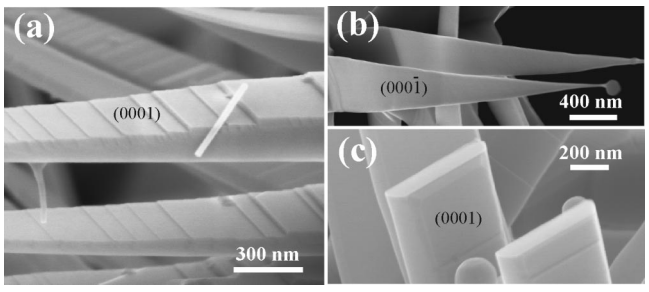

FIG. 4. (a) Front view of two individual blades, showing surface steps; (b) back side view of the bottom surfaces of nanoblades, showing smoother surface; (c) trapezoid cross section of a nanoblade.

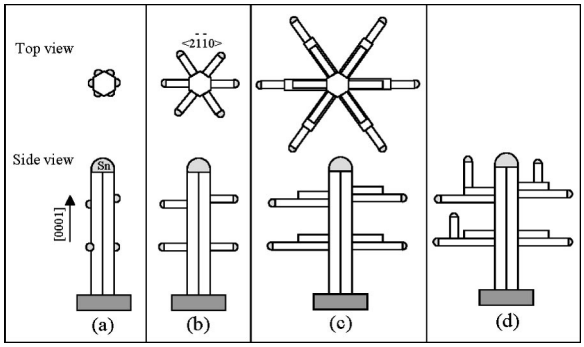

FIG. 5. Schematic growth process of the nanoblade arrays. The diagram shows only one column of nanopropeller array for simplicity of illustration.

cross section [Fig. 4(c)], indicating that the side surface is not exactly (0110). The shorter width side of the trapezoid corresponds to the stepped top surface, while the longer side to the flat bottom surfaces.

The growth of ZnO is dominated by the vapor–liquid–solid (VLS) process guided by the Sn catalyst[9,14,15] and by the self-catalysis process.[16] ZnO nanobelts have been grown without using catalyst, and ZnO can be self-catalytic.[16] Initially, the ZnO and SnO_2 powders were reduced by graphite and vaporized in the form of Zn, ZnO, Sn, and O vapors. In a lower temperature zone, Sn vapor condenses onto the substrate, which lead to the growth of ZnO nanowires along [0001] and enclosed by {2110} surfaces[11] [Fig. 5(a)]. This is a fast growth process. The Sn vapor which condensed later on the surface of the nanowire lead the epitaxial growth of ZnO nanobelts out of the surface of the nanowire, which extends along the six radial directions: $\pm$[2110], $\pm$[1120], $\pm$[1210], forming the hexagonal symmetric nanoblades [Fig. 5(b)]. The nanoblades also grow transversely along $\langle 0110 \rangle$ as the growth proceeds along $\langle 2110 \rangle$, resulting in growth steps towards the tip [Fig. 5(c)]. The latter condensed Sn droplets on the surface of the nanoblades lead to the growth of secondary nanowires along c axis [Fig. 2(b)], and this growth is along $+c$ axis rather than $-c$ axis due to higher catalytic activity of the Zn-terminated basal plane, which will be discussed next.

The growth morphology depends on the local temperature, surface diffusion rate, and availability of Zn–O vapor. In a lower temperature region, a relatively slower surface diffusion and the decrease in supply of the vapor as more source material being consumed, a triangular-shape structure is formed. On the other hand, a transverse growth along $\langle 1010 \rangle$ can extend the width of the nanoblades as the growth proceeds along $\langle 2110 \rangle$, resulting in the formation of triangular nanoribbon blades [Fig. 3(b)]. In the medium temperature region, a faster diffusion of the Zn–O vapor and higher surface mobility may lead to the formation of uniform and longer nanoblades [Fig. 3(c)]. By the same token, a faster growth along $\langle 2110 \rangle$ forms longer nanoblades in a higher temperature zone [Fig. 3(d)].

The c plane of ZnO is a polar surface, with Zn-terminated (0001) and oxygen-terminated (0001). Our recent study has found that the (0001)-Zn surface is chemically active in growing nanostructures, but the (0001)-O is inert.[16] Therefore, further growth along [0001] is possible on the top surface of the nanoblade, resulting in secondary growth of nanowires [Fig. 2(b), see Fig. 5(d)] as well as the formation of growth steps, but the (0001)-O bottom surface is flat without growth although Sn particles may be deposited on the surface. The reason for the formation of the trapezoid shaped cross section of the nanoblade [with shorter side on (0001)] and surface steps is likely due to a continuous growth along [0001], because the growth tends to reduce the area of the (0001) surface to decrease the surface energy due to polarization, resulting in a shrinkage in the width of the nanoblade along [0001].

In conclusion, this letter presents a two-step high temperature solid-vapor deposition process for synthesis of polar surface dominated ZnO nanopropeller arrays. The axis of the nanopropellers is a straight nanowire along the c axis and enclosed by {2110} surfaces; the sixfold symmetric nanoblades are later formed along the crystallographic equivalent a axes ($\langle 2110 \rangle$) perpendicular to the nanowire. The top surface of the nanoblade is the Zn-terminated $+c$ plane, showing surface steps and possible secondary growth of nanowires, while the back surface is the oxygen-terminated $-c$ plane, which is smooth and inert.

This work is supported by NSF (DMR-9733160) and NASA Vehicle Systems Program and Department of Defense Research and Engineering (DDR&E).

[1] K. Keis, L Vayssieres, S. Lindquist, and A. Hagfeldt, Nanostruct. Mater. **12**, 487 (1999).
[2] C. R. Gorla, N. W. Emanetoglu, S. Liang, W. E. Mayo, Y. Lu, M. Wraback, and H. Shen, J. Appl. Phys. **85**, 2595 (1999).
[3] T. Shibata, K. Unno, E. Makino, Y. Ito, and S. Shimada, Sens. Actuators, A **102**, 106 (2002).
[4] H. M. Lin, S. J. Tzeng, P. J. Hsiau, and W. L. Tsai, Nanostruct. Mater. **10**, 465 (1999).
[5] S. C. Minne, S. R. Manalis, and C. F. Quate, Appl. Phys. Lett. **67**, 3918 (1995).
[6] M. H. Huang, S. Mao, H. Feick, H. Q. Yan, Y. Y. Wu, H. Kind, E. Weber, R. Russo, and P. D. Yang, Science **292**, 1897 (2001).
[7] Z. W. Pan, Z. R. Dai, and Z. L. Wang, Science **291**, 1947 (2001).
[8] J. J. Wu, S. C. Liu, C. T. Wu, K. H. Chen, and L. C. Chen, Appl. Phys. Lett. **81**, 1312 (2002).
[9] P. X. Gao and Z. L. Wang, J. Phys. Chem. B **106**, 12653 (2002).
[10] J. Y. Lao, J. G. Wen, and Z. F. Ren, Nano Lett. **2**, 1287 (2002).
[11] P. X. Gao, Y. Ding, and Z. L. Wang, Nano Lett. **3**, 1315 (2003).
[12] X. Y. Kong and Z. L. Wang, Nano Lett. **3**, 1625 (2003).
[13] X. Y. Kong, Y. Ding, R. S. Yang, and Z. L. Wang, Science **303**, 1348 (2004).
[14] R. S. Wagner and W. C. Ellis, Appl. Phys. Lett. **4**, 89 (1964).
[15] Y. Ding, P. X. Gao, and Z. L. Wang, J. Am. Chem. Soc. **126**, 2066 (2004).
[16] Z. L. Wang, X. Y. Kong, and J. M. Zuo, Phys. Rev. Lett. **91**, 185502 (2003).